3.4 Injection System

3.4.1 Introduction

The injection system must provide the sources of electrons and positrons for the two linac beams. The low energy beams must be accelerated to 3.2 GeV where, if their emittance is not sufficiently small, they must be sent to damping rings for further emittance reduction in the x- and y-planes by synchrotron radiation damping. After the damping rings the beams proceed through bunch compressors and are injected into the main linacs.

For the positron source it is planned to use the "spent" high energy electron beam after it passes through the collision point in the interaction region. This beam is passed through a wiggler and the photons produced impinge on a rotating disc target where the resulting electromagnetic shower yields the required positrons. The positrons are focused in a solenoid and pre-accelerated to about 200 MeV in a normal conducting RF-structure. After that the beam is injected into a superconducting 3 GeV linac similar to the one used at the TTF. Since the damping ring is layed out for a normalized transverse acceptance of 0.05 m and and energy acceptance of $\pm 0.5\,\%$, the pre-linac must provide transport and acceleration of beams of at least this admittance.

The wiggler photon production scheme potentially can be modified to provide polarized positrons by using a helical undulator. This scheme is considered as an upgrade option.

The electron source is much more straightforward than what is needed for positrons. Even so, at this juncture there are several options and technical challenges to address. These hinge on the ability of an RF-gun to produce (a) sufficiently small and asymmetric ($\epsilon_y \ll \epsilon_x$) emittances, (b) polarized beams. The first issue can be resolved by having a damping ring for the electrons as well as the positrons. Concerning the second issue, if polarized beams are not possible with an RF-gun, then DC-guns are a reasonable backup. The following discussions will amplify these issues.

Once the electron beam has been produced and accelerated to a few MeV, it can be further accelerated in a 3.2 GeV injector linac similar to the TTF superconducting linac and either sent to the damping ring or passed directly through the bunch compressor to the main e^- linac.

3.4.2 Unpolarized Electron Source

The recent developments and efforts on laser driven RF guns make them attractive to consider for the electron source. The TTF Injector II can be used as a model for this type of injector. The injector II layout consists of the gun system followed by a single Tesla cavity and a magnetic bunch compressor (chicane). Various diagnostics and optical elements for beam analysis and matching into the TTF linac follow the chicane. The gun system consists of a laser, a normal conducting 1 1/2 cell L band gun cavity, and a focusing solenoid system. The present injector being developed for TTF uses a symmetric gun and should provide normalized emittances of $20 - 30 \cdot 10^{-6}$ m and bunch lengths of about 1 mm for bunch charges of 8 nC ($5 \cdot 10^{10}$ particles). The momentum spread needed for the bunch compression is about 250 keV. The bunch train consists of 800 bunches spaced at 1μs intervals for a macropulse length of 0.8 ms. The design has also been looked at for 1 nC and is expected to provide $< 5 \cdot 10^{-6}$ m emittance.

Laser systems being developed for the injector must provide stable intensity and phase light pulse trains as this determines the injection phase and charge variations of the bunches in the linac. The desired light pulse is flat temporally with 10-30 psec full width. Spatially, for the symmetric gun, a flat disk of 1.5-3 mm radius is required.

Two different laser systems under development use Nd:YLF flash lamp pumped lasers at 1054 nm with fourth harmonic generation to 263 nm for the photocathode illumination. The energy delivered to the photocathode per bunch is 5-10 μJ. The bunch to bunch energy stability is expected to be better than 10%.

The gun uses a photocathode of Cs_2Te. This cathode has a relatively long operating lifetime (months) at high quantum efficiency. Efficiencies as high as 3-5% are typical. Therefore for 10 nC out of the gun, at 1% efficiency and 4.7 eV photon energy the light pulse energy required per bunch is 5 μJ.

The gun photocathode is prepared (Cs_2Te coated on a molybdenum cathode plug) in a separate chamber and a number of cathodes can be interchanged without breaking vacuum of the gun system. An operating vacuum of 10^{-10} mbar is required.

The symmetric gun under development for TTF is a copper one and one half cell disk structure with a waveguide input on the full cell. Space charge emittance compensation is implemented with focusing solenoid lenses surrounding the gun. A field strength of 1.2 T is used. The peak RF field gradient is 35 MV/m for design operation. This is approximately the field on the cathode as well. The cavity iris radius is 20 mm, the shunt impedance Z = 28 MΩ/m, and RF peak power 2.2 MW. The beam energy out of the gun is about 4 MeV. It is hoped to be able to operate the gun at gradients as high as 50 MV/m which would require 4.5 MW RF peak power and provide better emittance quality.

The gun is followed by a cryostat with one 9-cell cavity to increase the energy to 15-20 MeV. Downstream of this cavity a magnetic chicane bunch compressor decreases the bunch length by about a factor of two to σ_z=1 mm. This injector system is designed to allow measurements of HOM losses and wakefields in the TTF cavities.

The superconducting pre-linac would look basically like the TTF linac. For an energy of 3.2 GeV, 120 9-cell cavities (15 modules) are required and the total length of the pre-linac is about 180 m.

3.4.3 Polarized Electron Source

At present, all operating polarized electron sources are using DC-guns generating long pulses in the ns range, usually followed by a bunching system (see e.g. [1]). A GaAs cathode is illuminated by suitable laser pulses to extract pulses of polarized electrons.

RF gun An attractive source of electrons here is the use of an RF gun rather then a dc gun. Rf guns have produced short bunches with high charge similar to the bunches required for TESLA. At the TTF [2] an injector for unpolarized electrons is under construction, which uses an L-band RF gun. So far, GaAs was not used in RF guns. One reason was the high sensitivity of the activated GaAs to contaminations [3]. An ultra-high vacuum of better than $1{\cdot}10^{-11}$ mbar must be maintained, which is not the case for existing RF guns. Suggestions have been made to overcome this problem leading to a first proposal using RF guns as a source for polarized electrons [4]. A successful attempt has recently been made to test a GaAs crystal in an RF gun [5]. Other potential problems when using GaAs as a cathode material have to be considered as well (see also [5]): the space charge and current density limit, multi bunch effects, the response time, the quantum efficiency and the laser system.

Space charge limit The space charge limit for short bunches can be estimated by Gauss' law for infinite separated electrodes: $\sigma = \epsilon_0 E$ with σ being the charge density on the cathode. For a reasonable extraction field E of 40 MV/m the extractable charge density is limited to 35 nC/cm^2, which is well above the requirements for Tesla.

Current density limit A more severe limitation specific to GaAs-type cathodes is the so called "cathode charge limit" [6], which is in the case of short excitation pulses practically a current density limit [5]. This limitation is typical for semiconductor cathodes with a negative electron affinity (NEA) surface, where a high electron extraction probability is achieved by the application of alkalis and oxides to the surface of the GaAs crystal. The NEA surface (together with the p-dopant, which bends the energy bands downwards at the surface) lowers the vacuum level below the conduction band minimum in the bulk, resulting in high extraction rates. The limit can be understood as a competition between the rate of near-thermal electrons arriving from the conduction band at the surface and the discharge rate of electrons from the surface [7].

Since the current density limit would increase with the discharge rate from the surface, it is preferable to use the highest possible extraction field. Also a larger cathode surface and longer pulses will lower the current density.

Because the maximum acceleration field in an RF gun varies linearly with the RF frequency, an S-band gun would be preferred. But on the other hand, the dimensions of an RF gun scale inversely with the RF frequency. Therefore, the maximum usable cathode area varies quadratically with the RF wavelength favoring L-band guns.

The current density limit for the Tesla case can be estimated using SLC data [8]: the SLC gun produces about 10 nC in a 2 ns long pulse from a cathode of an area of 1.5 cm^2 close to the cathode charge limit. A 100 nm medium-doped ($5{\cdot}10^{18}$/cm^3) strained-lattice GaAs cathode layer is used. The acceleration voltage is 1.8 MV/m. Thus, the current density is limited to 3.3 A/cm^2. Since the current density scales linearly with the acceleration voltage E [9], it is convenient to express the current density limit for the Tesla case (with bunch charge of 6 nC) by the following expression

$$E \;\; A \;\; \sigma_t \geq 3.3 \mathrm{A/cm}^2 \tag{3.4.1}$$

with E in MV/m, the cathode surface A in cm^2 and the FWHM pulse length σ_t in ns. Table 3.4.1 shows examples of combinations of E, A and σ_t for which the current density is at the limit of 3.3 A/cm^2, as measured at the SLC gun. For an L-band gun, several parameter sets fulfill the condition 3.4.1. A reasonable choice is an acceleration field of 40 MV/m and a pulse length of 26 ps with a cathode radius of 1 cm, which is not too large. The radius of the iris of an L-band gun is around 2 cm. It is not completely impossible to find a parameter set for an S-band gun, but one has to choose all the parameters at their limits. An L-band gun is clearly the prefered choice.

E [MV/m]	A [cm^2]	σ_t [ps]	remarks
40	3.1	26	reasonable L-band choice
40	13	6	largest cathode L-band
40	2.1	40	longest pulse length L-band
50	3.1	21	highest field L-band
70	2.5	20	S-band: all parameters at limit

Table 3.4.1: *Shown are examples of parameter sets, for which the current density is at the limit of 3.3 A/cm^2 as measured at the SLC gun. E is the accelerating voltage, A the cathode surface, and σ_t the pulse length (FWHM).*

Multibunch operation For multibunch operation, there is an additional effect of the cathode charge limit: the temporary flattening of the bands in the band bending region due to trapped electrons in the surface states, preventing further electrons from being extracted. Experiments at the SLC have shown, that the recovery time of the cathode is in the order of 10 to 100 ns depending on the cathode thickness [1]. This is much less than the Tesla bunch spacing of 708 ns.

Response time The response time of NEA cathodes is usually large. The theoretical model described in [7], which is consistent with SLC data, gives an estimation of 20 ps to 7 ns. Experiments indicate response times as low as 10 ps for cathodes with a thin layer of 150 nm [10].

Polarization, quantum efficiency and lifetime A polarized electron beam is produced by applying circular polarized laser light on a strained lattice GaAs cathode. SLC data show a polarization maximum of more than 80 % at a laser wavelength of 845±10 nm [11]. Unfortunately, the quantum efficiency drops sharply for highest polarization to 0.1 ... 0.3 %. In addition, the quantum efficiency depends strongly on the operating conditions of the gun. High dark current of more than 50 nA [1] and poor vacuum conditions reduces the quantum efficiency significantly. In addition, activation of the cathode by cesiation is regularly required. To obtain a reasonable up time of the source, a loading system which enables loading and removal of the cathode without breaking the gun vacuum is essential. Conditioning of the gun, regular cesiation and other cathode manipulations will be done with the cathode removed. A similar system will be tested for the TTF RF gun.

The SLC gun is operated with the same cathode for more than a year with a quantum efficiency between 0.1 and 0.3 % at highest polarization. The regular cesiation required to maintain this efficiency is done in situ without breaking the vacuum [11].

Laser Most polarized electron sources use lasers based on Ti:Sapphire, which are commercially available, especially for cw and pulsed applications with low repetition rates of a few tens of Hz. These lasers are tunable in a wide range around 800 nm and exceed easily the power or pulse energy requirements for most sources.

In our case, a long train of 0.8 ms length of 1130 bunches has to be generated with a repetition frequency of 5 Hz. This is very unusual for common lasers and requires a special design, which is not yet commercially available. For the TTF RF gun, such a laser system is under construction [2]. For the unpolarized source at TTF the requirements on the laser wavelength are different. Therefore, this laser will provide a test of the generation of the bunch train, but can not directly be used for a polarized source [12].

For the generation of long pulse trains, a laser material with good thermal properties like low thermal lensing is preferred. The strong thermal lensing of Ti:Sapphire would lead to a variation of the focusing of the laser beam during the pulse train resulting in an undesired non-uniformity. Other laser materials, which are tunable in the required wavelength range are Cr:LiCAF and Cr:LiSAF. Their advantage is the low thermal lensing and the possibility to be pumped by flash lamps and laser diodes [13]. Mode locked Cr:LiSAF lasers and regenerative amplifiers have been successfully built [14]. In the proposal for the TTF laser system, a laser based on Cr:LiSAF/Cr:LiCAF, which would fulfill the energy and bunch structure requirements, has already been discussed [15].

Emittance The emittance can be estimated using the formulae given in [16]. The thermal emittance scales linearly with the cathode radius. For a cathode radius of 1 cm one gets $\epsilon_{\mathrm{th}} = 5\,\pi\mathrm{mm\,mrad}$. The RF contribution to the emittance growth is larger, it scales quadratically with the cathode radius: $\epsilon_{\mathrm{rf}} = 10\,\pi\mathrm{mm\,mrad}$. Assuming that emittance dilution due to space charge can be largely compensated, the total emittance is expected to be below $20\,\pi\mathrm{mm\,mrad}$.

DC gun Studies have been made for a design of a high charge dc gun which meets the Tesla requirements in terms of bunch charge and train structure [17]. The proposed injector consists of a 500 kV electron gun followed by a bunching system. The emittance achieved was in the order of 200 to $300\,\pi\mathrm{mm\,mrad}$, which is well in the acceptance of the damping ring.

The previous discussion concerning the use of a GaAs cathode in such a gun, namely the charge limit, multi bunch operation, polarization, quantum efficiency, and laser is similar for the RF and dc gun option.

The main difference to an RF gun is that the acceleration field is much lower in a dc or pulsed dc gun. This limits the extractable beam current such that for the required charge of 6 nC the bunch length has to be in the ns scale. In addition, due to high space charge forces, the emittance is very large.

Let us consider the proposed 500 kV gun and a gun similar to the inverted-geometry gun proposed for SLC [18] which operates at 200 kV.

The current limit of a dc gun due to space charge can be estimated using Child-Langmuir's law. Taking a typical perveance of $0.3\,\mu\mathrm{A/V}^{3/2}$, the current is limited to 100 A for a 500 kV gun and 27 A for a 200 kV gun.

Scaling the cathode charge limit seen by the SLC gun to a field at the cathode of 10 MV/m for the 500 kV gun and 3 MV/m for the 200 kV option, the extractable current is then limited to $18\,\mathrm{A/cm}^2$ and $5.5\,\mathrm{A/cm}^2$, respectively. Taking a large cathode area of $3\,\mathrm{cm}^2$, the current is limited to 54 A and 16 A resp, which is lower than the limit due to space charge.

The required bunch charge for Tesla is 6 nC. Allowing a charge overhead of a factor of 2, the bunches must be longer than 250 ps and 750 ps, respectively.

A shorter bunch length is preferred, since it would simplify the bunching system. On the other hand, to avoid damaging of the cathode by ion bombardment, the dark current should be kept as low as possible. Besides a careful processing of the gun this requires low fields at the electrodes. The SLC gun operates at 120 kV with a dark current of less than 50 nA. The highest field on the electrodes is 7 MV/m [1]. The 500 kV gun designed for the TJNAF-FEL uses a GaAs cathode and will operate with fields of about 12 MV/m at the electrode surfaces [19].

As mentioned above, the gun vacuum has to be better than 10^{-11} mbar to allow a long cathode lifetime and thus a reliable operation of the gun. Processing and conditioning of the gun must be done without the cathode in place. A loading system will be attached to the gun, which allows loading and removal of the cathode without breaking the vacuum. This is also necessary for regular cesiations which will be performed at the removed position. A transport chamber will allow to insert a cathode prepared in a separate preparation chamber.

3.4.4 Flat Beam RF Photocathode Electron Source

The expected performance of cylindrically symmetric RF photoinjector systems is well understood from theoretical analysis and simulations which have been benchmarked by experiment. An extension to a fully three-dimensional approach has recently been undertaken by investigators at UCLA and Fermilab. This effort has been motivated by the demands of the TESLA linear collider design, in which the normalized emittances are $\epsilon_{x,y} = 14,\ 0.25$ mm mrad at Q = 5.8 nC. In this machine it may be possible to have asymmetric emittances at the injection point of an electron linac which meet the constraints set by the interaction point. In this way, the electron damping ring may be unnecessary, and in the case of $e-\gamma$ or $\gamma-\gamma$ collider options, no damping rings at all are needed. While the emittances may not be low enough to eliminate the need for an electron damping ring in the TESLA design under consideration, benefits in design and operation of the damping ring may be derived from injection of lower, asymmetric emittance electron beams.

To simply state the approach to design of an asymmetric RF photoinjector source [20], one uses the fact that the temperature of the emitted beam particles from a photocathode is only a function of cathode material and laser photon energy. This allows creation of asymmetric emittances $\epsilon_y \ll \epsilon_x$ by illuminating the photocathode with a ribbon laser pulse ($\sigma_y \ll \sigma_x$). Typically, the dominant emittance growth mechanism at relevant current densities is space-charge. This is conveniently mitigated by the ribbon geometry of the electron beam pulse. One must also pay attention to the potential for RF induced emittance growth, especially in the horizontal dimension where the beam is large. In the spirit of the problem for cylindrically symmetric systems performed by K.J. Kim [21], we have examined the scaling of emittances with respect to beam dimensions, accelerating gradient and phase, and beam charge. The "thermal" contribution to the emittance given by the finite spread in transverse momenta of photoemitted electrons is, assuming 0.1 eV emission temperature (typical of semiconductors)

$$\epsilon^{th}_{x,y}[mm \cdot mrad] \approx \sqrt{\frac{kT_\perp}{m_e c^2}} \cdot 0.25\sigma_{x,y}[mm] \tag{3.4.2}$$

For TESLA this implies beam sizes of $\sigma_x < 5\,\text{cm}$, and $\sigma_y < 1\,\text{mm}$.

Under the assumptions of a cylindrically symmetric RF cavity structure, it is easy to derive the minimum RF contribution to the rms emittances which arise from the time dependent transverse focusing forces in the RF structure; they can be simply written as

$$\epsilon^{rf}_{x,y} \approx \frac{eE_{rf}}{\sqrt{8}m_e c^2} \cdot \sigma^2_{x,y}(\Delta\Phi)^2, \tag{3.4.3}$$

where $\Delta\Phi = (\omega_{rf}/c)\sigma_z$ is the phase extent of the beam. Minimizing these quantities implies operation at low frequency, low accelerating gradient, and with small bunch sizes in all dimensions. For our case, we are considering a fairly large horizontal beam size as well as high gradient, and so this is an issue for the horizontal emittance.

There are a number of proposed ways to remove or minimize the emittance diluting phase dependent defocusing due to the transverse RF forces in the gun. Because of the use of emittance compensation to deal with the space-charge contribution to the emittance, it is perhaps wisest to use a scheme which mitigates the transverse kick in the x-direction. This can be accomplished by removing as best as possible the dependence of the RF fields on x. It should be noted in this regard that the defocusing kick induced at the end of a cylindrically symmetric cavity has approximately equal electric and magnetic parts. The electric component of the kick is mainly due to the fringing fields near the iris at the exit of the gun. The fringe field can be made mainly vertical simply by making the iris opening a slit, long in the horizontal dimension. The magnetic component, however, cannot be so easily diminished, as it is not dependent on the iris, but the accelerating field in the interior of the cavity. The only way to diminish the magnetic force in the horizontal direction is to break the symmetry of the cavity outer wall. The simplest asymmetric structure is a rectangular box cavity, but this only diminishes (does not eliminate) the horizontal RF forces, and produces a sinusoidal dependence of the accelerating field on the x-dimension. A better choice is to use an "H-shaped" structure, which has been investigated in the context of sheet-beam klystron development at SLAC. In this structure, the accelerating field in the "bar" region of the H-cavity has no dependence on x and therefore has acceleration independent of transverse position, as in a symmetric structure. It should be noted that the vertical forces (which are due mainly to the backwards speed-of-light space harmonic in this p-mode structure) in this case in the bar region are now entirely in the vertical dimension, and are twice as large as the equivalent symmetric cavity. The function of the side regions is to allow the longitudinal field to go zero sinusoidally, to satisfy the boundary condition, and choose (along with the vertical dimension) the cavity resonant frequency. An example of this structure, along with the fields that it supports are shown in Fig. 3.4.1, which displays the results of a 3-D electromagnetic simulation for a 2856 MHz cavity under development at UCLA, using the code GDFIDL [22].

An analysis of the space-charge contribution to the emittance gives the following scaling, derived from both approximate analysis and PARMELA simulation [20]:

$$\epsilon_{x,y}^{sc} \approx \frac{2N_b r_e}{7\sigma_{x,y}W}\exp(-3\sqrt{W\sigma_y})\sqrt{\sigma_y/\sigma_z}, \qquad W = \frac{eE_{rf}\sin(\Phi_0)}{2m_e c^2}. \tag{3.4.4}$$

Here, the scaling $\epsilon_x^{sc} = (\sigma_x/\sigma_y)\epsilon_y^{sc}$ is approximately obeyed; this is a consequence of the fact that for an ellipsoidal charge distribution, the normal electric field at any bunch boundary is approximately the same. It should be noted that minimizing the space charge contributions to the emittances implies operation at high accelerating gradient. It should also be emphasized at this point that these emittances, induced by the space charge at low energy, are mainly due to the different orientations of each "z-slice" of the beam. A scheme is discussed below, emittance compensation, which can remove these correlations, effectively lowering the emittances of the bunch. Before taking up this discussion, it should also be pointed out that one cannot arbitrarily reduce σ_y, because of the limit on surface charge density emitted from the cathode before the retarding space-charge cuts off emission ($\sigma_x\sigma_y > 2Q/E_z$). This effect has been observed at UCLA.

It is instructive to look at the product of the emittances, to see if there is some chance of achieving the desired emittances without need for emittance compensation,

$$\epsilon_x^{sc}\epsilon_y^{sc} \approx \left[\frac{2N_b r_e}{7W}\right]^2 \cdot \frac{\exp(-6\sqrt{W\sigma_y})}{\sigma_x\sigma_z}. \tag{3.4.5}$$

The argument in the exponential in this expression is generally smaller than one for reasonable accelerating gradients, and so one can see that in general a beam large in the longitudinal and horizontal dimensions is needed to minimize the product of the space charge emittances. Unfortunately, these are precisely the dimensions that the RF contributions are sensitive to, and thus one cannot consider making them arbitrarily

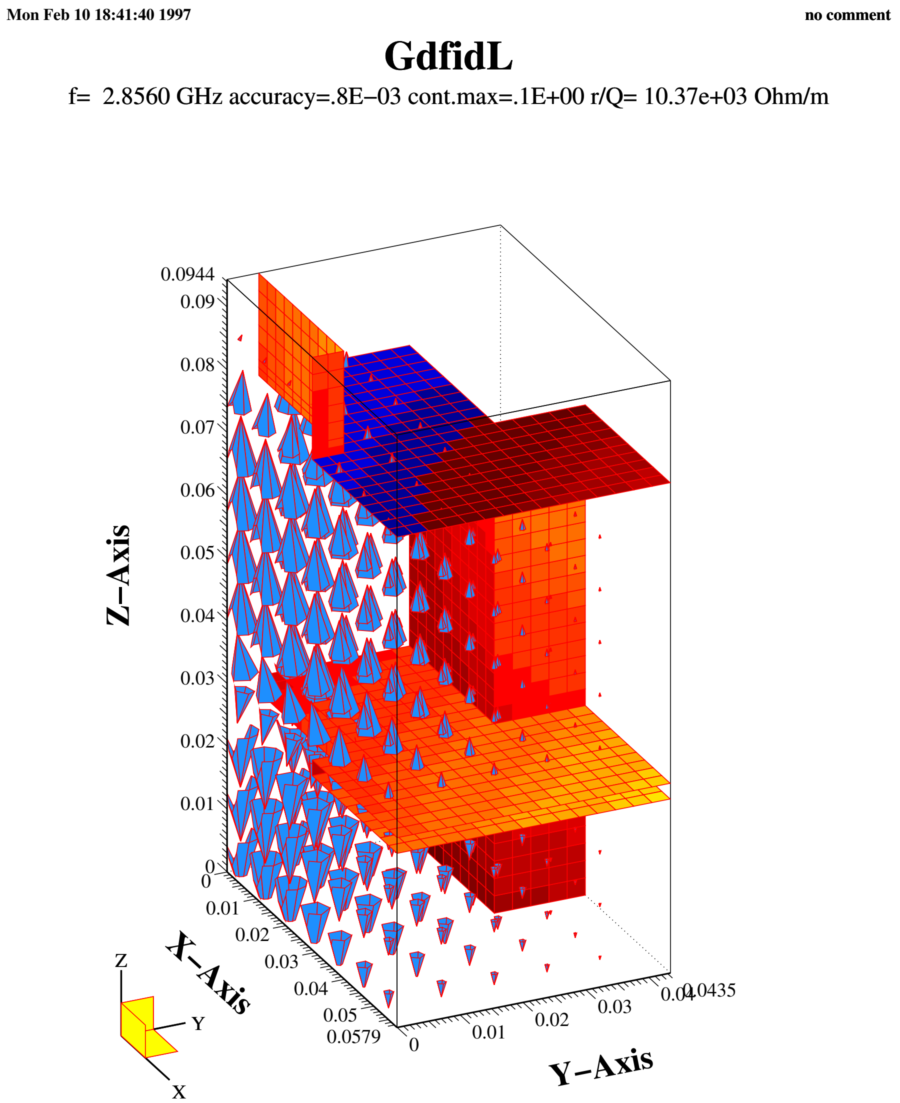

Figure 3.4.1: *Three-dimensional electromagnetic simulation of S-band, H-shaped asymmetric RF gun structure, from program GDFIDL.*

large. As an example of a design where the RF contribution is not yet significant, we take $N_b = 3.6 \cdot 10^{10}, W = 80m^{-1}, \sigma_z = 2mm, \sigma_x = 2.5cm, \sigma_y = 1mm$. In this case, we have $\epsilon_x \epsilon_y \approx 600(mm \cdot mrad)^2$ as opposed to about $3(mm \cdot mrad)^2$ as needed by TESLA, and we miss the design goal by an order of magnitude in both dimensions.

It is apparent that further efforts must be made in order to achieve the emittances needed for linear collider designs, that is, one must employ an emittance compensation scheme for sheet beams accelerated in asymmetric RF structures. Emittance compensation is essentially a process by which the correlations (mainly as a function of the longitudinal position in the bunch) in the beam transverse phase space that are induced by space charge forces in the photocathode gun, are removed by focusing the beam, and allowing the correlations to be removed after one surface-plasma oscillation of the space-charge dominated beam. When the orientation of the transverse phase space ellipse of each "z-slice" has the same angle, the linear component of the emittance due to this effect is removed. Since the space-charge forces must still be large enough after the focusing lens to allow for compensation, this scheme tends to work better at lower accelerating gradients for convenient focusing geometries. This fortunate direction in the design of the system allows us to mitigate concerns about the RF contribution to the emittance, and about peak and average RF power (source and heat dissipation problems), in both the symmetric and asymmetric cases. In the asymmetric case, we must have the RF contribution to the transverse phase space trajectories be small, otherwise the space charge compensation will suffer from interference. This condition is achieved by the choice of large aspect ratio (sheet) beam profile, and the asymmetric structure described above.

While the serious design calculations must be performed with simulation programs which include as many experimental effects as possible, these are very time consuming. One needs to have a model which predicts the approximate behavior of the system before proceeding to simulation. This has been developed recently as an extension of the analytical understanding of the emittance compensation process [23]. This process proceeds by first focusing and then accelerating, in order not to "freeze out" emittance oscillations, as previously conjectured, but to drive down the emittance in a secularly diminishing fashion. This behavior is obtained when one operates on the invariant envelopes, which are analogous to the Brillouin flow obtained in a non-accelerating system. In the case of asymmetric beams, one must break the symmetry of the external focus in order to suppress a quadrupole oscillation which tends to immediately symmetrize the x- and y-beam envelopes. This can be done by using a vertically focusing quadrupole field super-imposed on the final acceleration section (solenoidal focusing is not allowed in this device, because of a coupling of the x and y phase planes due to an $\vec{E} \times \vec{B}$ rotation which is dependent on longitudinal position in the beam), such that the quadrupole strength is chosen as

$$K_x = -\frac{1}{4}\left(\frac{\gamma'}{\gamma}\right), \tag{3.4.6}$$

where γ' is the average normalized accelerating gradient in the linac.

In order to illustrate this process, we show the results of a calcuation which integrates the envelope equations for a number of different z-slices, at positions z_i. The transverse focusing forces arise from external quadrupole focusing, and from the first order transient kicks experienced by electrons at the exit and the entrance of the RF cavities, and the second order (alternating gradient focusing) in the interior of the RF cavities. Emittance terms included in the envelope calculations are only the thermal components.

The results of a typical calculation are shown in Fig. 3.4.2. In this case, the vertical emittance is well compensated, while there is essentially no improvement in the horizontal emittance. This is because the effective defocusing strength associated with the space charge is different in the two dimensions, as can be seen from the envelope equation,

$$K^{sc}_{x,y} = \frac{4I(z_i)}{I_0\gamma^3(\sigma_x + \sigma_y)\sigma_{x,y}}. \tag{3.4.7}$$

Because of this, the compensation process generally proceeds much faster in the small dimension, and thus it is difficult to design a system which simultaneously compensates in the vertical and horizontal dimensions.

The solution to this problem is straightforward: since the beam near the cathode is much larger in x than in y or z, one can effectively remove the dynamics in the x direction (and the dependence on x of the y and z components of the space charge forces), as it is already done for the RF contributions, from consideration by making the beam distribution uniform in x. The effect of this is illuminated by Fig. 3.4.3, which displays the x component of the force along the x- axis of the bunch, and the y component of the force at one σ_y, in the $y-z$ plane, for two cases: (a) where the beam distribution is gaussian in all three dimensions, and (b) where it is gaussian in y and z , but uniform up to a hard boundary in x . It can be seen that for the trigaussian beam the horizontal forces rise approximately linearly to a large value at about one σ_x. For the uniform distribution in x, however, there is very little horizontal field over about 85-90% of the beam, and the field rises steeply and nonlinearly near the beam boundary. As it was noted before, the maximum field is nearly the same, but the region of the beam which is affected is much smaller. Note that the vertical field is also nearly uniform over almost all of the beam, again degrading near the beam edge. In practice, one uses this final 10-15% of the beam as "guard charge" during the compensation to remove the horizontal field and homogenize the vertical field, then removes it by collimation after the linac section. In this way, one effectively removes the x-dimension from the compensation problem, reducing the problem to two dimensions, as in the (by now well understood) cylindrically symmetric case. It should be noted in this regard that the multiple envelope model for emittance compensation dynamics has been compared extensively to simulation as well as to the analytical model of Serafini and Rosenzweig [23], and has been essentially validated for cylindrically symmetric beams. Benchmarking of the models in the asymmetric case awaits further refinements of three-dimensional computational tools. Point-by-point simulations with PARMELA have displayed emittance compensation, but proven too noisy and time-consuming to explore the physics in detail. A three-dimensional particle-in-cell code for modelling this type of photoinjector is presently under development at UCLA, which should be better able to predict the performance limitations of this device quantitatively.

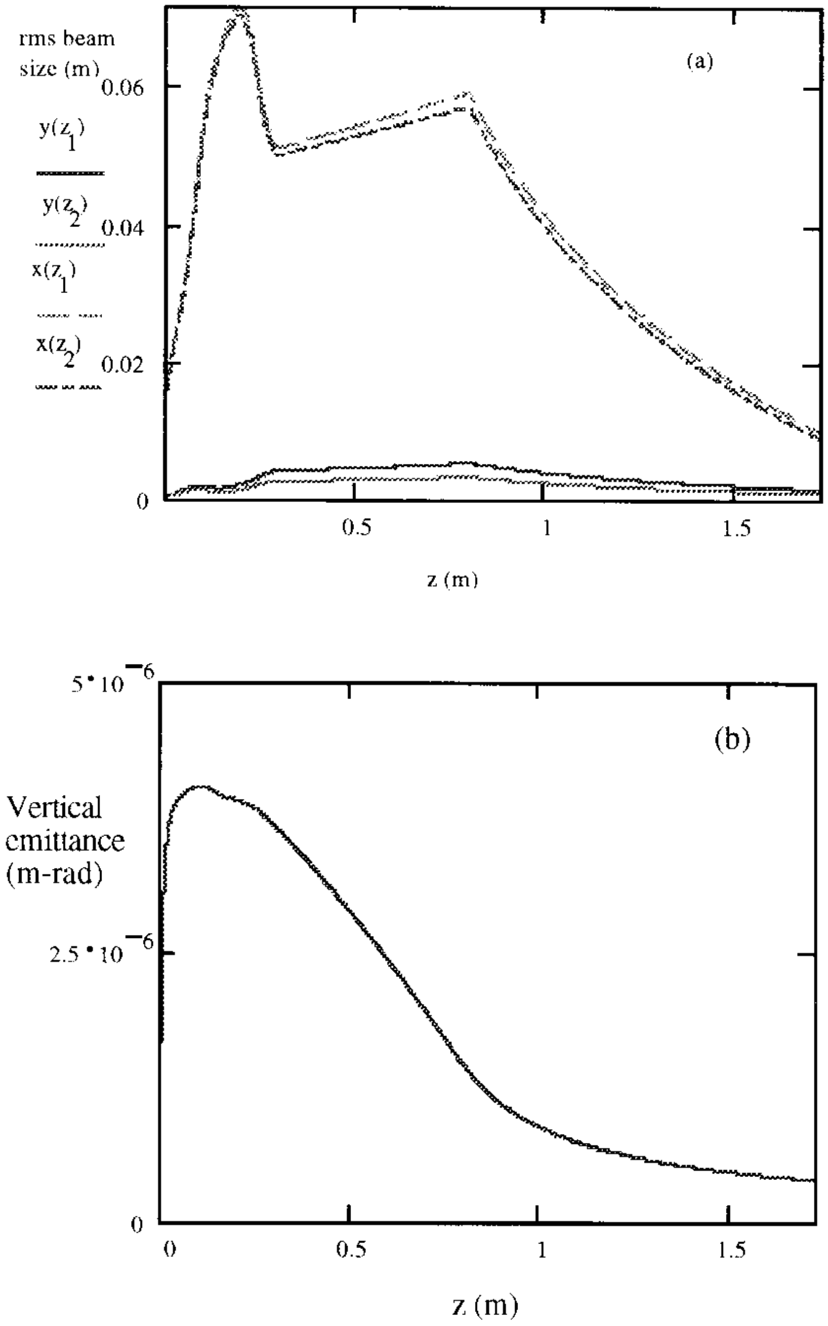

Figure 3.4.2: *(a) Rms beam sizes for two beam slices in multiple-slice model calculation of emittance compensation for 10 nC beam. A vertically focusing quad is placed symmetrically over the cathode plane, followed by a horizontally focusing quad, another doublet, a drift, and a TESLA cavity linac. (b) Vertical emittance evolution in this case.*

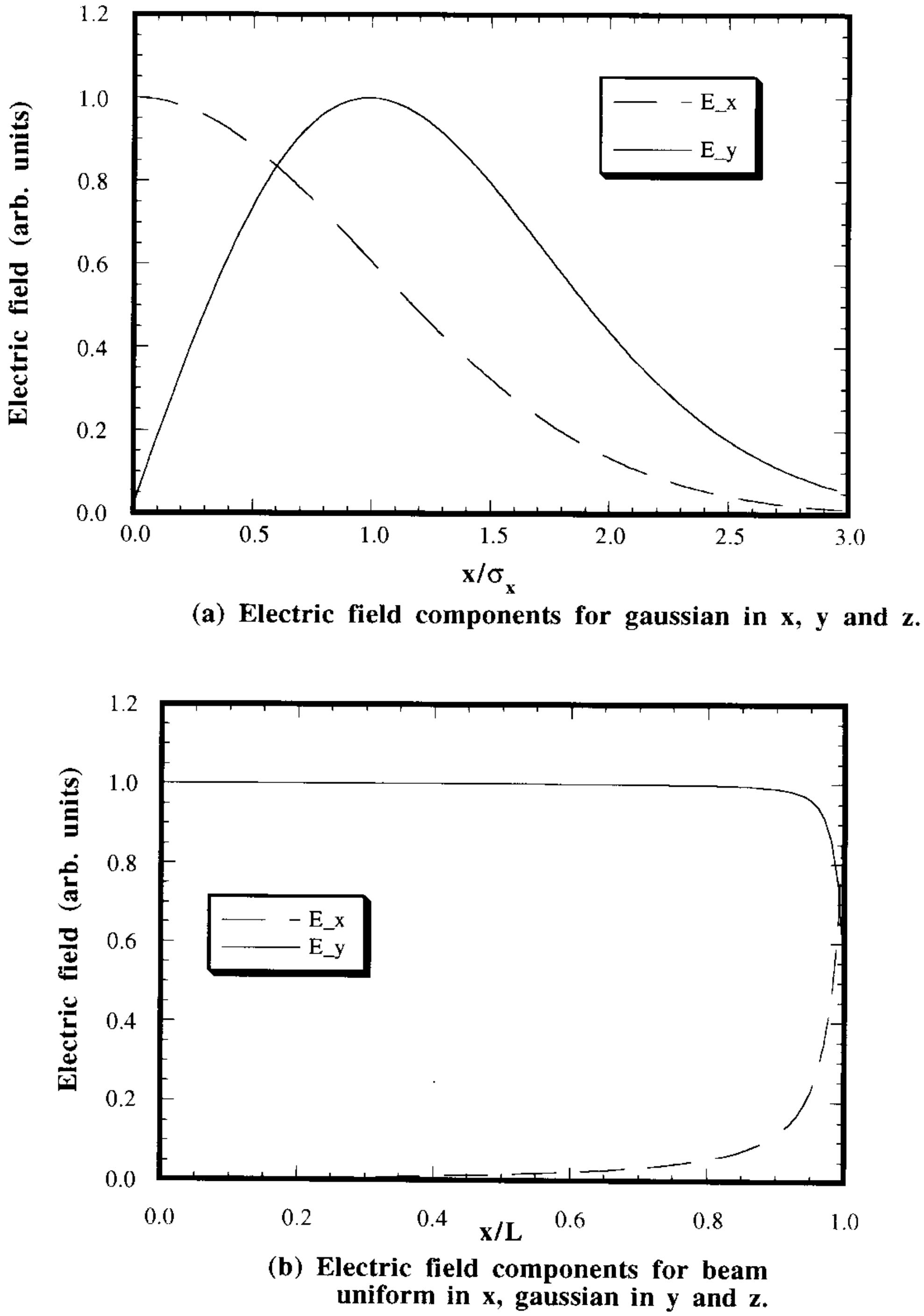

Figure 3.4.3: *Electric field components for (a) uniform, as opposed to (b) horizontally gaussian density profile.*

3.4.5 Positron Source

3.4.5.1 Introduction

A fundamental intensity limit for positron sources is given by the thermal stress which is built up in the conversion target due to the energy deposition of the primary electron beam. In case of TESLA the bunch train is so long that the target can be rotated even within the bunch train. With a target velocity of 50 m/s the heat load of about 50 bunches contributes to the thermal stress at a given position of the target. Table 3.4.2 compares the design parameters of TESLA with parameters reached at the SLC positron source which is the positron source with the highest intensity operating so far.

The SLC source is operating close to the stress limit of the target. An extension of this kind of source by two orders of magnitude in intensity seems to be impossible with a reasonable effort of technological development. Therefore a new concept based on the conversion of high energy wiggler radiation in a thin target has been developed [24, 25]. The scheme allows also to produce polarized positrons but the technological demands for a polarized source are higher than for an unpolarized source. The present design is for an unpolarized source but allows for a later upgrade to produce polarized positrons.

parameter	SLC	TESLA
# of positrons p. pulse	$3...5 \cdot 10^{10}$	$4.1 \cdot 10^{13}$
# of bunches p. pulse	1	1130
pulse duration	3 ps	0.8 ms
bunch spacing	8.3 ms	708 ns
repetition frequency	120 Hz	5 Hz

Table 3.4.2: *Comparison between TESLA and SLC parameters.*

3.4.5.2 General Layout

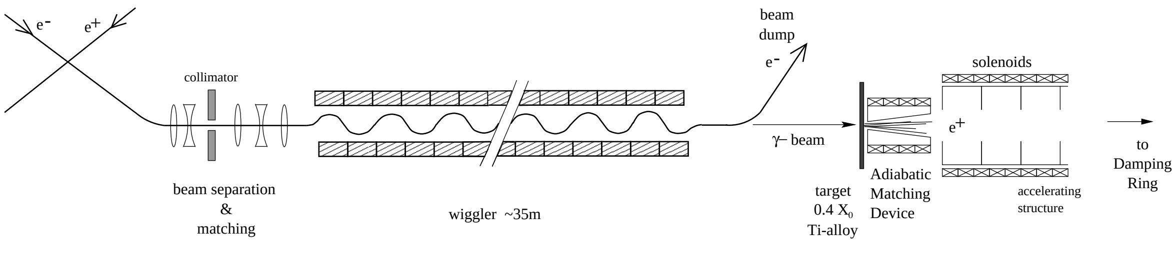

Figure 3.4.4: *Sketch of the positron source layout.*

A schematic layout of the source is shown in Fig. 3.4.4. The source is designed to produce twice as many positrons as required. The 250 GeV electron beam is used after collision as primary beam for the positron production. Due to the strong beam-beam forces during the interaction process the emittance of the beam is increased and the energy distribution has developed a long tail of low energy particles. The outgoing electron beam is separated from the incoming positron beam and then collimated in order to remove the low-energy tail. Still more than 80% of the particles pass through the optics (see next section). The final beam emittance is $\epsilon_x < 10^{-8}$m and $\epsilon_y < 10^{-9}$m, sufficiently small to match the beam to the successive wiggler section. The wiggler is a conventional design of 35 m length. Here photons are generated with a broad energy distribution extending up to above 70 MeV. A dipole section of $\approx$30 m length separates the electron beam from the photon beam and guides it to the beam dump. The photons are used to produce electron-positron pairs in the thin conversion target. A minimum spot size of the photon beam on the target of σ_{min}=0.5 mm can be realized. The heating of the target is dominated by the ionization losses of electrons and positrons given by $E_{dep} \approx 2\text{MeVcm}^2/\text{g}$ per charged particle. Thus the temperature rise of the target ΔT can be estimated as:

$$\Delta T[K] = \frac{2eN \cdot 2 \cdot 10^6}{c \cdot A \cdot \eta} \tag{3.4.8}$$

where c denotes the heat capacity in $Jg^{-1}K^{-1}$, A the source area in cm^2 and η the efficiency of positron capture after the target. In order to get N positrons, $2N/\eta$ particles (electrons and positrons) have to emerge from the target. The heat load of the target is determined by three more or less free parameters:
- the heat capacity of the target material c,
- the efficiency of the capture optics η,
- the source area A.

An increased source area counteracts a high capture efficiency, because the phase-space density of the emerging positrons is reduced, thus a small source area is favorable. Since in the present design the photons are generated in a wiggler, rather than by bremsstrahlung in the target, a high positron yield is reached with a thin target of only 0.4 radiation length (X_0) thickness. Compared to a conventional source the thermal stress of the target can be significantly reduced by two effects:
- one is able to use a material with low nuclear charge Z which in general have a high heat capacity.
- the divergence of the positron beam is small due to the reduced scattering in the target and hence the capture efficiency is increased.

A conventional target requires many radiation lengths for the full development of the electromagnetic cascade. Positrons which are produced in the first steps of the cascade will not emerge from the target due to the ionization losses inside the material. The ionization loss per radiation length depends on the material and is lower for high Z materials. Hence a high-Z material has to be used in a conventional source in order to reach a high positron yield. In thin targets, however, the conversion efficiency is in first order independent of the material. Therefore it is possible to use a low-Z material which has a higher heat capacity (Dulong-Petit-rule). In the present design a Titanium alloy is foreseen as conversion target which allows to increase the particle density in the target by about an order of magnitude as compared to a high-Z Tungsten-Rhenium alloy.

The second advantage of a thin target is the reduced multiple scattering which determines the transverse beam emittance of the positrons. The rms scattering angle scales with the square root of the path length of the particle in units of X_0. The rms scattering angle scales non-linearly with the target thickness since in a conventional source most of the positrons are produced close to the target exit. Nevertheless, the transverse momenta of the positrons produced in a thin target are considerably smaller than the transverse momenta of positrons from a conventional source. Therefore the capture efficiency is increased by a factor 4-5 in the present design as compared to a conventional source.

The capture optics behind the target is of a conventional design. Since the positrons have a broad distribution of transverse and longitudinal momenta they have to be accelerated in an acceleration section embedded in a solenoid field. The acceptance of a solenoid channel is characterized by a large spot size and small angles while the positrons emerging from the target have a small spot size and large angles. To match the positrons to the acceptance of the solenoid, an Adiabatic Matching Device (AMD) is used. It consists of a tapered solenoid field which starts with a high initial field and tapers down adiabatically to the constant end field.

After acceleration to an energy of 150-200 MeV the positrons are separated from the electrons and the photons in a magnetic chicane. The electron and the photon beams are dumped and the positron beam is accelerated to its final energy and transferred to the damping ring.

The safety margin of a factor of two in the positron production rate is valid for 250 GeV electron beam energy. For operation at lower energy this margin is reduced. Without modifications, the source can be used down to about 160 GeV. Operation at lower energy with full design positron beam intensity requires to increase the length of the wiggler.

In the following the components of the positron source will be discussed in more detail.

3.4.5.3 Spent Beam Capture System

Due to the very strong beam-beam force the particles which do not pass through the center of the opposing bunch are strongly deflected. This disruption effect causes a broadening of the angular distribution after the interaction. The beam size remains nearly constant or even decreases due to the focusing pinch effect.

For all investigations a data set of roughly 12000 particles was created with a beam-beam simulation code using the parameters at the interaction point. Fig. 3.4.5 shows the phase space distributions both in the horizontal and vertical plane. The differences in the distribution are caused by the flatness of the beam.

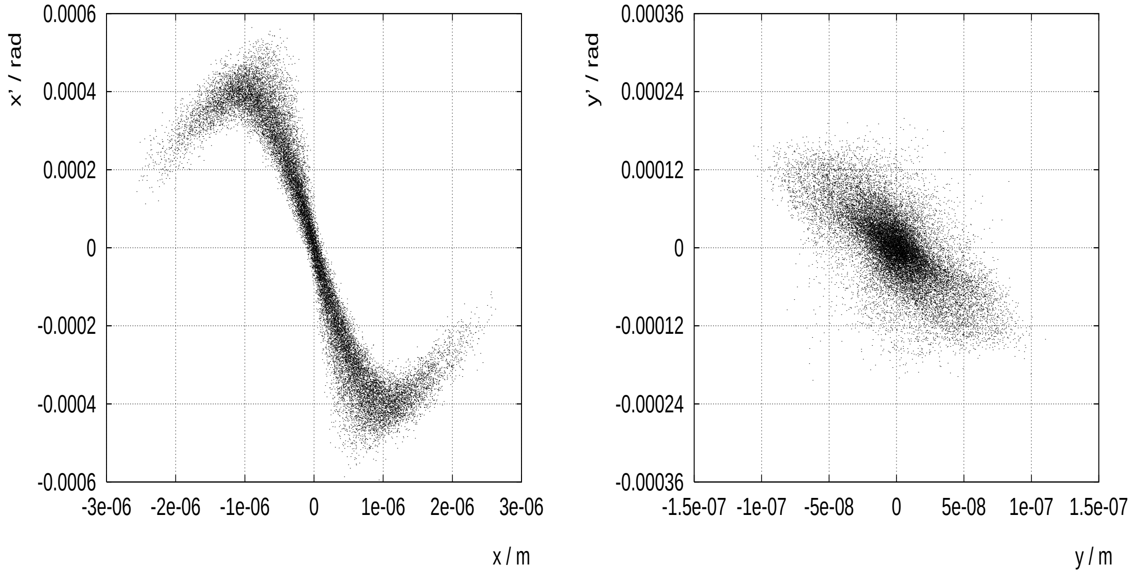

Figure 3.4.5: *Horizontal and vertical phase space distribution after the interaction.*

The deflected particles emit high-energy synchrotron radiation (beamstrahlung). This statistical process causes a broad energy spread of the disrupted beam and a mean energy loss of 3% of the initial energy. A non negligible part of the beam has lost more than 10% energy. Fig. 3.4.6 shows the energy distribution after the interaction.

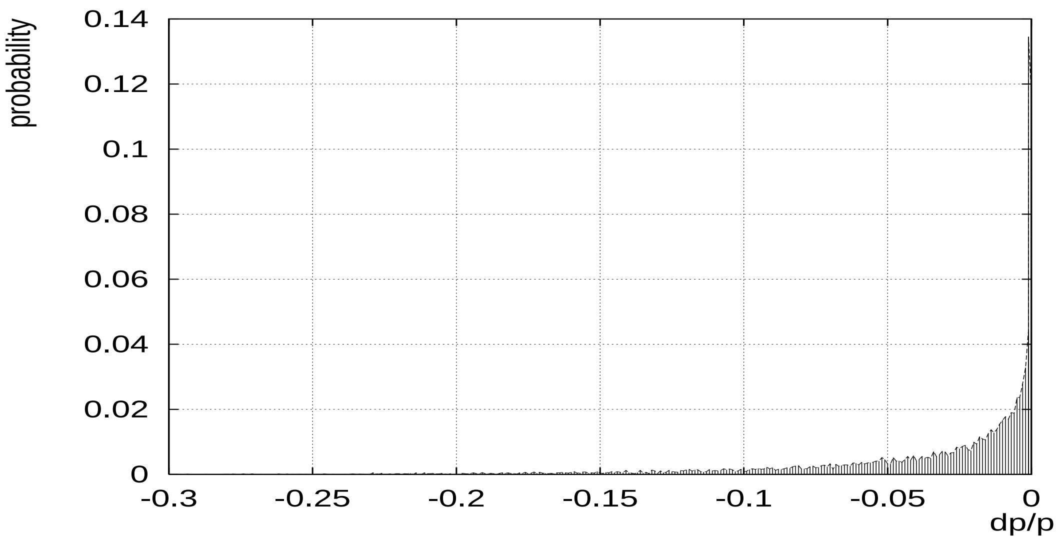

Figure 3.4.6: *Energy spectrum of the disrupted beam*

The spent beam is focused by the final doublet (FD) of the FFS for the incoming beam. As mentioned above the disrupted beam has a very small diameter and a broad angular spread. Thus the matched β-functions after the IP are small and are rising to very high beta values inside the FD. This yields strong chromatic effects which cause an emittance growth by three orders of magnitude horizontally and two orders of magnitude vertically if uncompensated. Since the vertical emittance after the interaction is about two orders of magnitude smaller than required, it is sufficient to compensate only the horizontal chromaticity in a chromatic correction system (CCS).

Chromatic Correction System

After initial separation of the spent beam as described in section 3.7 a magnet lattice basically very similar to the horizontal CCS for the incoming beam follows. The boundary conditions for the design of this beam-optical system are:

- The geometry of the beamline should be such that it fits together with the FFS into the same tunnel.
- The bending magnets have to be sufficiently weak to avoid strong emittance growth from synchrotron radiation.
- The momentum bandwidth has to be large to accomodate a large fraction of the broad momentum distribution of the spent beam.

Starting from a basic layout which fulfills the first two conditions an optimization of the bandwidth is performed by adding sextupoles at strategic positions in the lattice. An ensemble of representative trajectories is tracked through the system. Optimum sextupole strengths which lead to a minimum beam emittance at the end of the lattice are determined. The procedure is similar to the one applied in ref. [26]. The amount of spent beam accepted by the system is directly related to the maximum tolerable emittance in the wiggler. As shown in Fig. 3.4.8, the horizontal emittance starts growing rapidly if more than 85...90% of the beam is passed through the beamline, indicating that the low-energy tail falls outside the bandwidth of the optics. So even with an optimized achromatic system it is not possible to transport the whole beam from the IR on through the capture optics and afterwards through the wiggler or undulator. Thus the low energy tail which still contains a considerable fraction of the beam power has to be collimated.

After the end of the CCS the optics is continued with a drift space of 20m and two quadrupole doublets with a distance of 18.7 m. The beam is focused such that the radiation emitted in a 35 m long wiggler hits the target in a focal point 30 m behind the wiggler i.e. 70 m behind the last quadrupole doublet.

Fig.3.4.9 shows the geometry of the whole capture system with the wiggler and the drift space to the target with regard to the beam delivery system of the oncoming positron beam. The separation between the two beamlines is sufficiently small to fit into a tunnel of 5 m diameter.

The optimization of the optics and the need to collimate the major part of the low energy particles mainly in regions without optical elements (see tab.3.4.3) results in a capture efficiency of 84.3% of the disrupted electron beam.

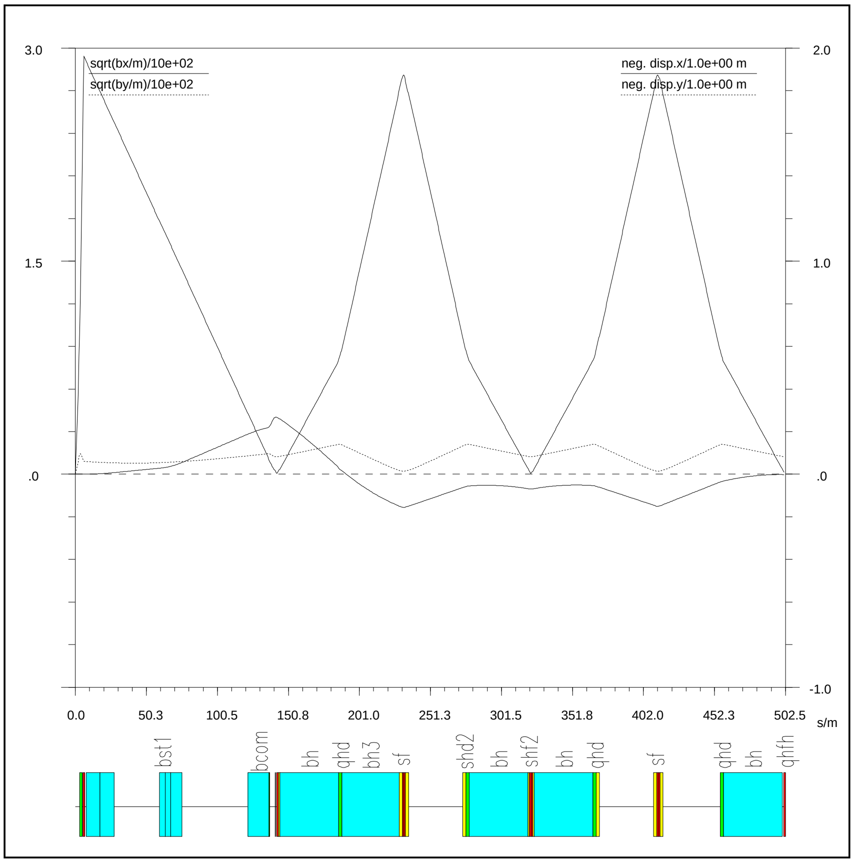

Figure 3.4.7: *Optics of the spent beam capture system.*

Although the rms-beamsize along the optics does not exceed values of 7 mm horizontally and 1mm vertically the maximum horizontal amplitudes can grow above 6 cm. To reduce the maximum horizontal beamsize a small fraction of the beam had to be collimated inside the second bending magnet in the first FODO cell. Fig. 3.4.10 and Fig. 3.4.11 shows the maximum beam envelopes of the disrupted beam along the capture optics with the position of the collimators. The 35 m long wiggler is positioned between 553 m and 588 m behind the IP.

Stability of the positron source

The efficiency of the capture optics for the disrupted electron beam depends on the parameters of the interacting bunches. The optics and the collimation system shown in Fig. 3.4.7 and Fig. 3.4.9 is developed for interacting bunches with design parameters. In reality, the capture efficiency for the disrupted beam may not be constant but depends on the energy spread due to beamstrahlung. As explained above, the beamstrahlung is a function of the bunch charge and other interaction parameters.

If we consider a perturbation of the interaction, for example a displacement of the orbit, the spent electron beam would not be disrupted like in a head-on interaction. Hence the number of captured electrons passing the collimation system can be higher.

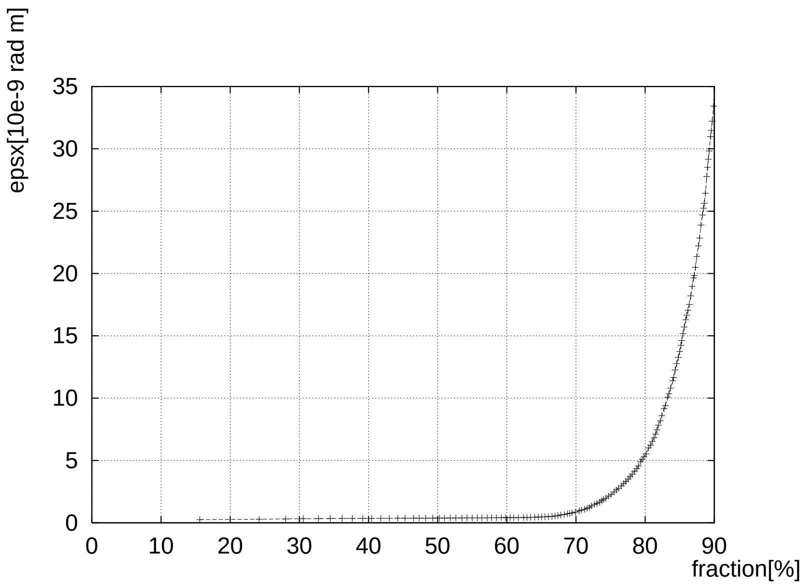

Figure 3.4.8: *Horizontal emittance at the end of the system vs. percentage of the captured spent beam.*

Collimator	Position behind IP [m]	Collimated beam power [KW]	Remarks
COL1	27.51-59.51	356.19	between the separator and the septa
COL2	75.51-122.12	372.52	between the septa and the first bend
COL3	188.64-229.14	74.6	inside the second bend in the 1st FODO cell
COL4	235.89-274.14	144.48	inside the CCS
COL5	502.52-522.52	212.33	after the CCS
COL6	547.74-552.74	1.88	5m before the wiggler to avoid vertical amplitudes $> 2\,\mathrm{mm}$

Table 3.4.3: *Collimator positions and collimated beam power.*

The positron bunches in the next pulse have a higher charge which in turn causes a higher electron beam energy spread after the IP. The fixed energy acceptance of the capture optics then leads to a lower intensity electron beam for the photon production. In the second pulse after the perturbation the positron bunch has a lower charge and so the system can oscillate. For a stable operation of the linac, this oscillation must be damped.

The investigation of stability is started with the maximum perturbation, i.e. the case that the bunches do not interact at all. The electrons pass the collimation system completely and the positron bunches for the next pulse have a 19% higher charge than

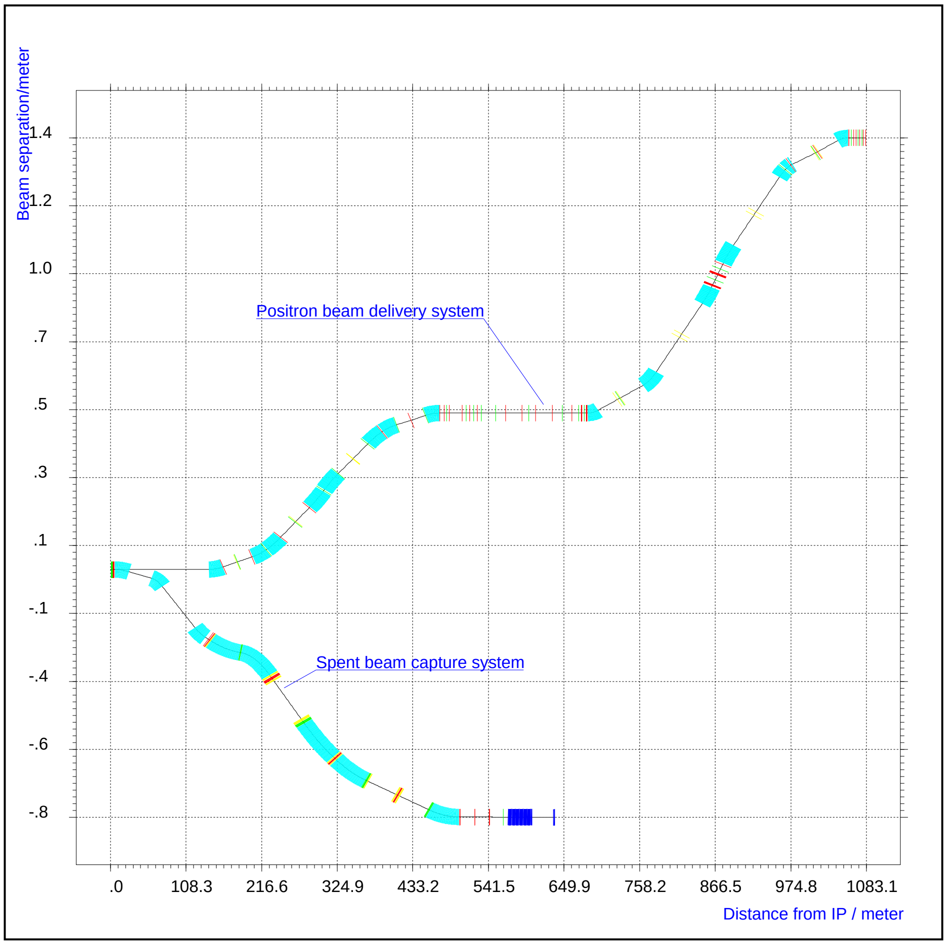

Figure 3.4.9: *Beam line for the disrupted beam with the 35 m long wiggler (lower branch) and the incoming positron beam (upper branch). At the end of the capture optics the separation is 1.3 m.*

designed. The next interaction is simulated with this asymmetric bunch charges. The outgoing disrupted electron beam was tracked through the capture optics to obtain the efficiency for the following pulse. This yields a new (reduced) positron intensity for the next interaction, etc. Fig. 3.4.12 shows the resulting behavior of the bunch charge as a function of interactions after the perturbation. The oscillation decreases and so the positron source can be operated stably from this point of view.

Efficiency Gain due to Parameter Change at the IP

The efficiency of the capture system is limited by higher order geometric and chromo-geometric aberrations. With a relatively moderate adjustment of the interaction parameters, both the horizontal beam emittance and the energy spread can be reduced, thus decreasing the population of the tails in the spent beam which have to be colli-

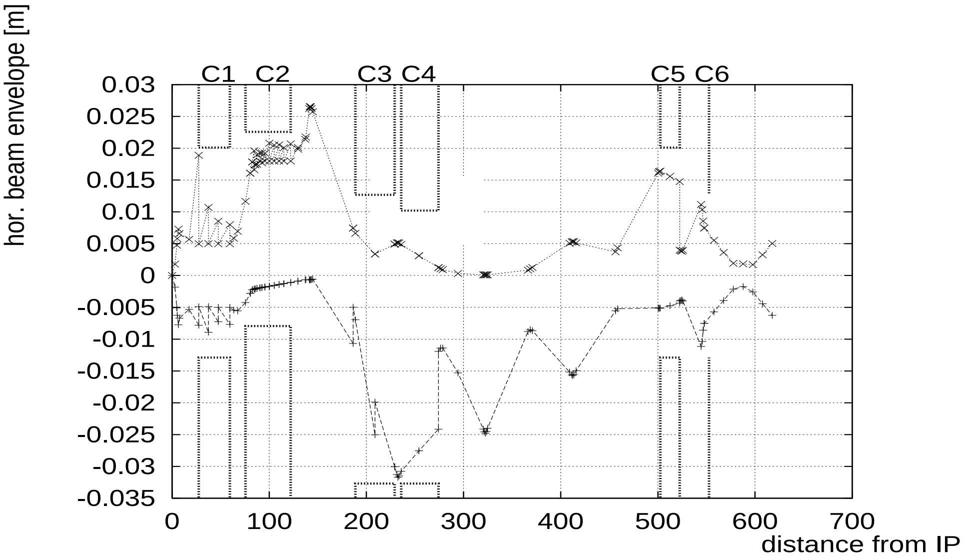

Figure 3.4.10: *Horizontal envelope for an ensemble containing 84% of the spent beam.*

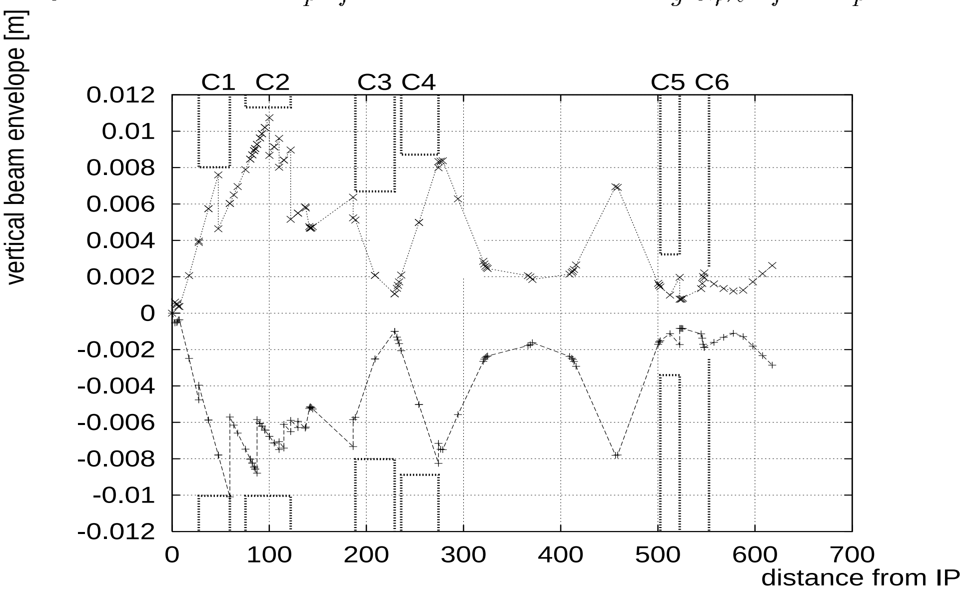

Figure 3.4.11: *Vertical envelope for an ensemble containing 84% of the spent beam.*

mated. This is demonstrated in Fig. 3.4.13 where the spent beam capture efficiency is shown as a function of the horizontal beta of the positron beam at the IP. An increase of $\beta_x^*(e^+)$ by a factor of two already reduces the amount of collimated spent beam from 16% to 6%. At the same time, the luminosity is reduced by only about 20%, which can be compensated by a slight reduction of the vertical beam emittance. With such a modification, the operation of the source becomes very insensitive with respect to fluctuations of the interaction parameters. Furthermore, an efficient operation of a polarized positron source would be greatly facilitated.

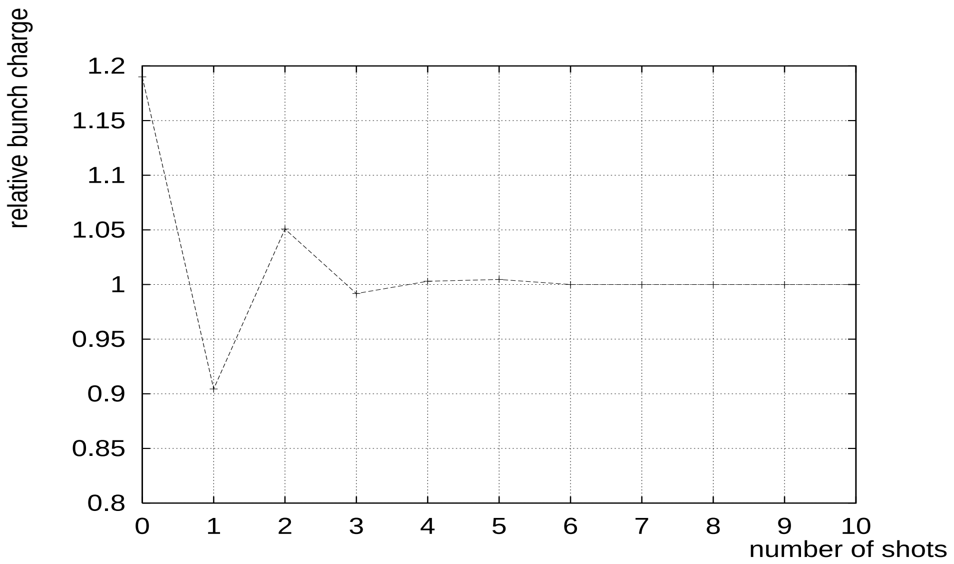

Figure 3.4.12: *Oscillations of the positron bunch intensity after one missing interaction. The bunch charge reaches the design value after 4 pulses.*

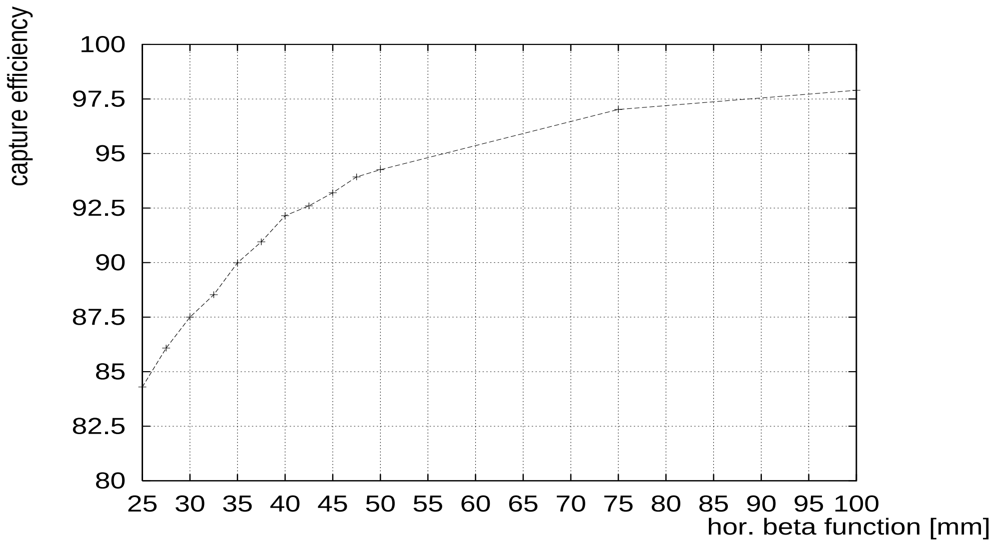

Figure 3.4.13: *Capture efficiency as a function of the horizontal β-function of the positron beam at the IP. Starting from the design value of 25 mm the capture efficiency reaches 97.9% of the disrupted beam for $\beta_x^*(e^+) = 100\,mm$.*

3.4.5.4 Wiggler

A planar wiggler consists of a row of short dipole magnets with constant field strength but alternating field direction. For a large period length λ_w the photon number spectrum can be approximated by the well known photon number spectrum of a dipole magnet. Fig. 3.4.14 shows the photon number spectrum of a 1m long dipole with a magnetic field of B=1.7 T.

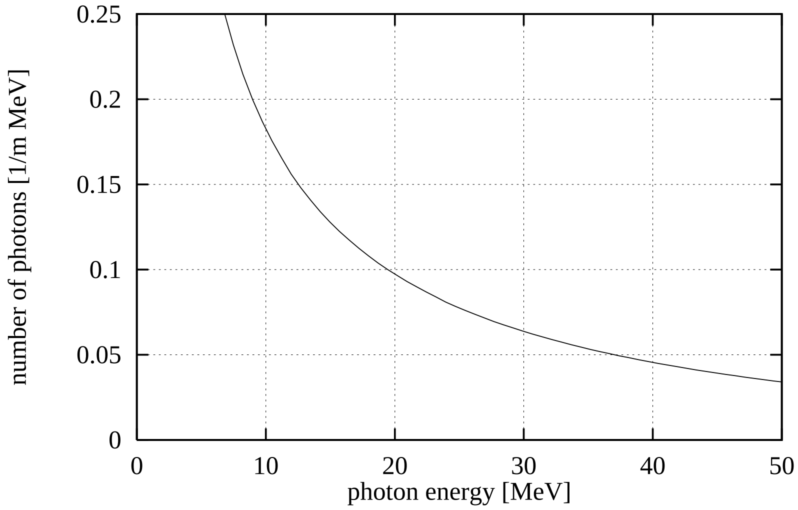

Figure 3.4.14: *Photon number spectrum of a planar wiggler with B=1.7 T at a beam energy of 250 GeV.*

In order to reach a small spot size of the radiation on the target the electron beam is focused through the wiggler onto the target. The contribution of the natural opening of the wiggler radiation to the spot size can be approximated by:

$$\sigma_{SR} \approx \frac{eB\lambda_w}{2\pi p_e} \cdot (L/2 + D) \qquad (3.4.9)$$

Here p_e denotes the electron momentum, L the wiggler length and D the driftspace between the wiggler and the target.

For $L \approx 35$ m and $D \approx 30$ m the period length λ_w should not exceed 3.2 cm in order to reach a spot size contribution of 0.5 mm. Since the electron beam emittance is quite small a gap height of only 5 mm is sufficient to transport the beam through the wiggler. Today wigglers and undulators based on permanent magnet technology are widely used in both synchrotron radiation sources and free electron lasers. Period length and magnetic fields similar to the values discussed above are not unusual for these devices. In contrast to the sinusoidal field distribution of a synchrotron radiation device a more rectangular distribution would be favorable for the positron source in order to keep the length of the wiggler shorter. Various inexpensive proposals of wigglers with a rectangular field distribution and similar period length are discussed in ref. [27].

3.4.5.5 Target

A high energy photon passing through a material can create an electron positron pair in the field of a nucleus (pair production). These charged particles again lose energy on their way through the material via collisions with electrons (ionization) and radiation processes in the field of a nucleus (bremsstrahlung). The ionization losses account for the majority of heat deposition in the material, while photons produced via bremsstrahlung may once more produce electron positron pairs. This sequence continues, i.e. the number of electrons, positrons and photons increases exponentially, while the mean energy of the particles decreases. The development of the shower decays when the particle energy drops below ≈10 MeV because the energy loss due to ionization exceeds the production of photons at low energies. Bremsstrahlung and pair production are essentially inverse processes, hence they can be characterized by a common parameter called the radiation length X_0. The radiation length of a material is approximated by:

$$X_0^{-1} = \frac{4\alpha r_e^2 N_A \rho}{A} \cdot Z(Z+1) ln(183 Z^{1/3}) \tag{3.4.10}$$

where A is the atomic weight, Z the nuclear charge, ρ the density of the material and N_A Avogadro's number.

Since for important electromagnetic processes (bremsstrahlung, pair production, multiple scattering) some or all of the dependence upon the medium is contained in the radiation length, it is convenient to measure the target thickness in terms of the radiation length. Besides bremsstrahlung and pair production the shower development is influenced by many other processes like Compton scattering, Møller scattering, Bhabha scattering, photo effect etc. A complete treatment of the development of an electromagnetic cascade is possible only with a numerical simulation code. The following calculations have been performed with the code EGS4 [28]. The EGS code is a general purpose package for the Monte-Carlo simulation of electromagnetic showers. Since its formal introduction in 1978 it has been extended and improved and a lot of comparisons with experiments have verified the performance.

Fig. 3.4.15 shows the positron yield per electron as function of the target thickness for different materials. The incoming photon beam has been generated in a 1m long wiggler of 1.7 T magnetic field. For a target thickness above $0.5X_0$ the yield increases slowly before it starts to decrease again. Since the multiple scattering increases the beam emittance with increasing target thickness, the optimum overall efficiency, i.e. including the capture efficiency, is found at about $0.4X_0$. At this thickness the yield for a low Z material like Titanium is only about 16% lower than for Tungsten.

In Fig. 3.4.16 the temperature distribution in a Titanium target induced by a single train of wiggler photons from a 35 m long wiggler of 1.7 T is shown. As a safety margin the number of positrons produced in this simulation exceeds the nominal value behind the capture optics by a factor of two.

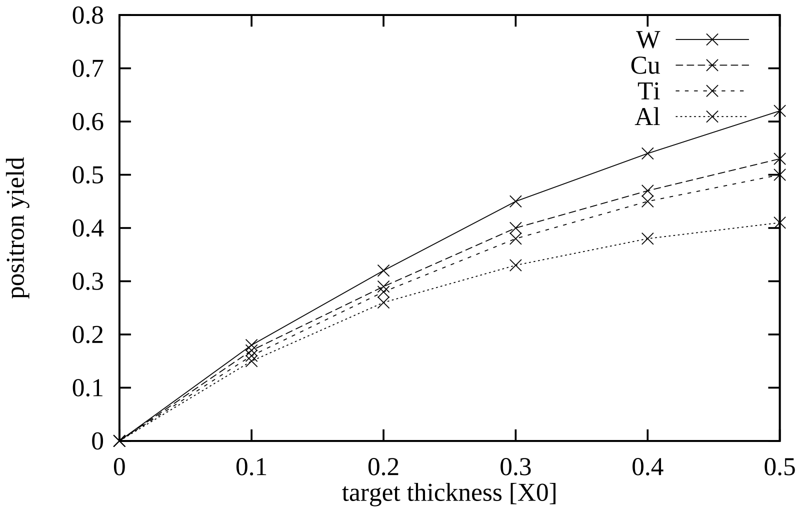

Figure 3.4.15: *Positron yield vs. target thickness for different materials. The photons are generated by a 250 GeV electron beam in a 1 m long wiggler of 1.7 T magnetic field.*

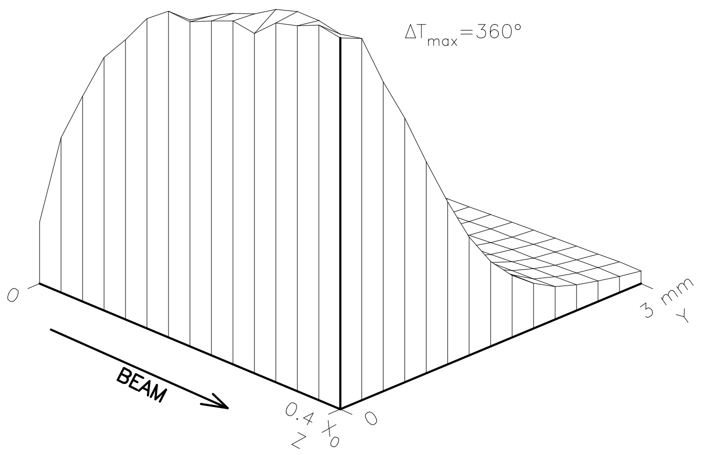

Figure 3.4.16: *Radial and longitudinal temperature distribution in the Titanium target. The spotsize of the incoming beam is $\sigma_{x,y}$=0.7 mm.*

The maximum temperature rise is only 360 °C, lower than the maximum temperature reached in a Tungsten-Rhenium target close to the stress limit given in ref. [29]. The density of charged particles is higher in the Titanium target but due to the 5 times higher heat capacity the temperature does not increase.

Besides the temperature rise the mechanical constants of the target material have to be taken into account. Experimental data for the maximum heat load of a low

Z positron conversion target are not available even though the material is used in high power collimators. In order to scale the results obtained for high Z targets to the case of low Z targets the material constants can be combined with respect to their proportionality to the mechanical stress $P_t \approx \Delta T \alpha E$ induced by heating (α: expansion coefficient, E: elastic modulus).

The induced stress has to remain below the 0.2% yield strength $P_{0.2}$ which is the stress where the deformation of a material ceases to be elastic, $P_t < P_{0.2}$.

Table 3.4.4 lists material constants for the Tungsten-Rhenium alloy used in the SLC positron source and various Titanium alloys.

The geometrical dimensions of the SLC target (thickness: 2.1 cm) and a Titanium target (thickness: 1.4 cm) are comparable while the temperature distribution in direction of the rotation of the target is quite different. The ratio $P_{0.2}/\alpha E = \Delta T_{crit}$ can be used to compare the maximum temperature rise that the target can withstand. It is seen from Table 3.4.4 that the maximum temperature in a Titanium target can be up to twice as large as in a Tungsten target.

material	c [J/kg]	α $10^{-6} K^{-1}$	E $10^{11} N/m^2$	$P_{0.2}$ $10^7 N/m^2$	ΔT_{crit} K^{-1}	x_0 cm	ρ g cm^{-3}
W-26Re	0.13	5.0	4.00	91.0	455	0.35	19.3
Ti	0.52	8.4	1.16	55.0	564	3.56	4.54
Ti-5Al-2.5Sn	0.52	9.3	1.17	86.3	793	3.5	4.46
Ti-13V-11Cr-3Al	0.62	8.8	0.98	96.1	1114	3.5	4.82

Table 3.4.4: *Material constant of Tungsten-Rhenium and various Titanium alloys.*

The target has to rotate with a high velocity in order to avoid an overlapping of all bunches within one RF pulse at the same target spot. A velocity of about 50 m/s at the circumference of the target is necessary to spread out the beam spot over a distance of 4 cm. This can be achieved with a target of 80 cm diameter rotating at 1210 revolutions per minute. The maximum heat load reached in this case corresponds to 50 bunches overlapping at the same location or a temperature rise of about 380 °C. The diameter of the target ring is chosen in a way that subsequent bunch trains are placed next to each other on the target so that all parts of the target ring are loaded equally. The average heat load amounts to 7 kW. Cooling by radiation might be sufficient in case of the large target wheel but needs further careful investigation. Cooling with water is possible with a vacuum feed-through based on differential pumping as it has been designed at CERN [31].

3.4.5.6 The Capture Optics

The particles which emerge from the target have to be accelerated in a cavity embedded in a solenoid field for focusing. Here the final emittance and the efficiency of the positron source are defined. Since, compared to the thick target of the conventional

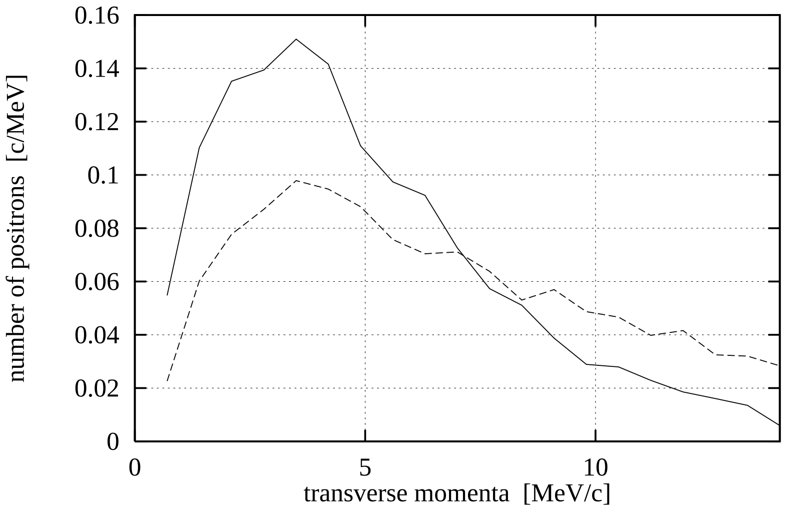

Figure 3.4.17: *Comparison of transverse momentum distribution for a SLC-like source ($6X_0$, W, dotted line) and a thin target as proposed here ($0.4X_0$, Ti, solid line).*

source the multiple-scattering is reduced in a thin target, the transverse momenta of the positrons emerging from the target are smaller. Fig. 3.4.17 compares transverse momenta of a SLC-like source with those of a thin target source driven by photons from a wiggler.

The smaller transverse momenta lead to a higher capture efficiency of the positrons behind the target. In order to match the emittance of the positron beam, characterized by a small spot size and a large divergence, to the acceptance of the solenoid which is determined by a large spot size and a small divergence a matching section is introduced between the converter target and the first accelerating cavity. The matching section consists of a so-called Adiabatic Matching Device (AMD), a tapered solenoid starting with a high initial field and tapered adiabatically down to the constant end field. The acceptance of the system is matched to the acceptance of the damping ring so that no particle losses occur later in the damping ring. Besides the acceptance of the damping ring that limits the useful acceptance of the matching device two mechanisms lead to an emittance growth of the positron beam in the matching device and hence to additional particle losses:
- emittance growth due to non adiabatic fields.
- bunch lengthening due to path length and velocity differences.
R. Helm has found a solution for the particle motion in an adiabatically varying solenoid field [32] from which he derived the optimum on-axis field distribution for the matching device along the longitudinal coordinate z as:

$$B(z) = \frac{B_i}{1 + g \cdot z} \tag{3.4.11}$$

where B_i is the initial solenoid field and g the taper parameter.

The condition for an adiabatic field variation is then given as $(gp_e)/(eB_i) \ll 1$. In order to fulfill this condition for particles with higher energy the taper parameter g has to be small. However, this means that the matching section becomes long and that the bunch lengthening becomes stronger. An optimum is reached with g=30 m^{-1} in the present design. Figure 3.4.18 shows the energy distribution of the positrons as they emerge from the target and the fraction of captured particles for the optimized optics. Figure 3.4.19 shows the longitudinal distribution of the positrons behind the AMD. While the core of the distribution represents the incoming electron beam (σ_z=0.7 mm or 1° of RF-phase), a long tail has developed due to bunch lengthening effects. The positrons in the tail will be lost in the damping ring since the curvature of the RF leads to a large energy deviation of these particles. In the simulation an energy acceptance of ±1 % corresponding to an RF phase of ±7.5° is assumed.

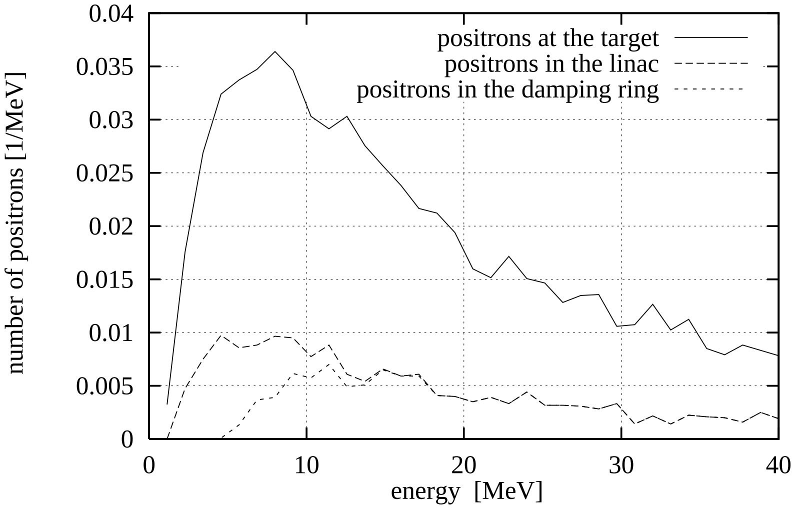

Figure 3.4.18: *Energy distribution of the positrons after the target (solid line) and the fraction of captured positrons (dashed lines).*

A capture efficiency of 17% can be reached with an initial field of 6 T. Fields of up to 8 T have already be realized [33] and 10 T seem to be feasible. However, since the bunch train is long the realization of a higher field is more difficult with a pulsed device and a lower field seems to be more reasonable. Table 3.4.5 collects important parameters of the positron source.

3.4.5.7 Positron PreAccelerator

The accelerating structure downstream of the positron source accelerates both positrons and electrons emerging from the titanium target. The number of electrons is 1.7 times that of the positrons. Both particles are accepted in the Adiabatic Matching Device

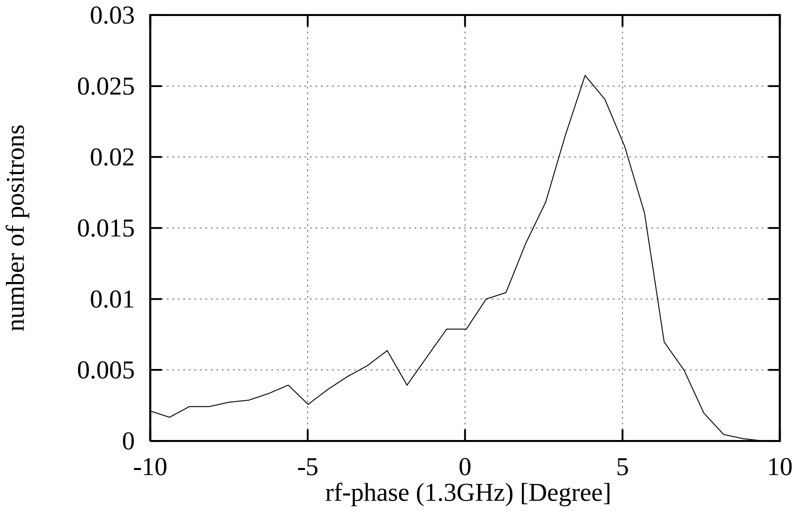

Figure 3.4.19: *Longitudinal beam profile of the positrons after the matching device.*

(AMD) where they undergo helical trajectories with identical characteristics, provided their energy and transverse momenta are the same. The only difference concerns the sense of rotation of the helical trajectories. The maximum transverse momentum, for particles moving close to the axis ($x_0 = y_0 \approx 0$), is about 3 MeV/c at the target and 0.5 MeV/c at the exit of the AMD. The corresponding maximum radius of the helix in a constant field solenoid surrounding the accelerator section is then approximately 10 mm. Hence positrons and electrons with the same transverse momentum are moving on helices with the same radius but with different path shifts, depending on their energy.

Energy differences between positrons and electrons

In an accelerating section optimised for positron acceleration, the electrons are first decelerated and then re-accelerated after having lost almost all of their kinetic energy. The energy difference between positrons and electrons, together in the first RF bucket at the entrance to the accelerating section reaches, therefore, about twice the average value of the energy of the electrons. This could be verified easily if the central energy of the accepted positrons in the Matcing Device is well defined. Experimental evidence of such behaviour has been observed at LAL-Orsay and CERN with a Quarter Wave Transformer as a Matching Device. Such a system, exhibiting a narrow energy acceptance makes the verification easier. In this case, at LAL as well as at LIL (CERN), the energy difference corresponded to twice the central energy associated with the matching system. We might then expect a similar behaviour for the electrons and positrons with an energy difference of about 15-20 MeV.

Choice of the pre-accelerator structure

The transverse and longitudinal acceptances for the positron source depend on the pre-accelerator parameters. Choosing a large iris aperture helps in improving the transverse

Wiggler	
peak field	1.7 T
period length	31 mm
gap height	5 mm
γ-spot size on target	0.7 mm
# of photons p. electron	368
mean photon energy	22 MeV
photon beam power	250 kW
Target	
material	Ti-alloy
thickness	1.42 cm ($0.4X_0$)
pulse temperature rise	360 K
av. power deposition	7 kW
Adiabatic Matching Device	
initial field	6 T
taper parameter	30 m^{-1}
end field	0.16 T
capture cavity iris radius	23 mm
General	
capture efficiency	17%
# of positrons p. electron	2
norm. e^+-beam emittance	0.01 m
total energy width	±30 MeV
required D.R. acceptance	0.048 m

Table 3.4.5: *Overview of the positron source main parameters.*

acceptance; however, bunch lengthening due to particle spiralling in the longitudinal magnetic field is made easier in large apertures. The limitation in bunch lengthening is imposed by the limitations on energy dispersion at the entrance of the Damping Ring (DR). Figure 3.4.20 shows the acceptance region in the (pL, pT) phase plane. The borders are defined as follows; - Energy: $(p_L)_{min}, (p_L)_{max}$

- Transverse momentum: $(p_T)_{max}$

- Bunch lengthening: Angular limits are represented for the case of S-band and L-band structures and for a maximum RF phase spread of 15 degrees.

Here the energy domain is given between 5 MeV and 25 MeV, the maximum transverse momentum at the target is about 6 MeV/c (3 MeV/c for near axis particles). It can be seen that in order to maximise the overall acceptance for the positron source an L-band structure with a rather large iris is preferable. This frequency choice (1.3 GHz) also matches with the main linac frequency.

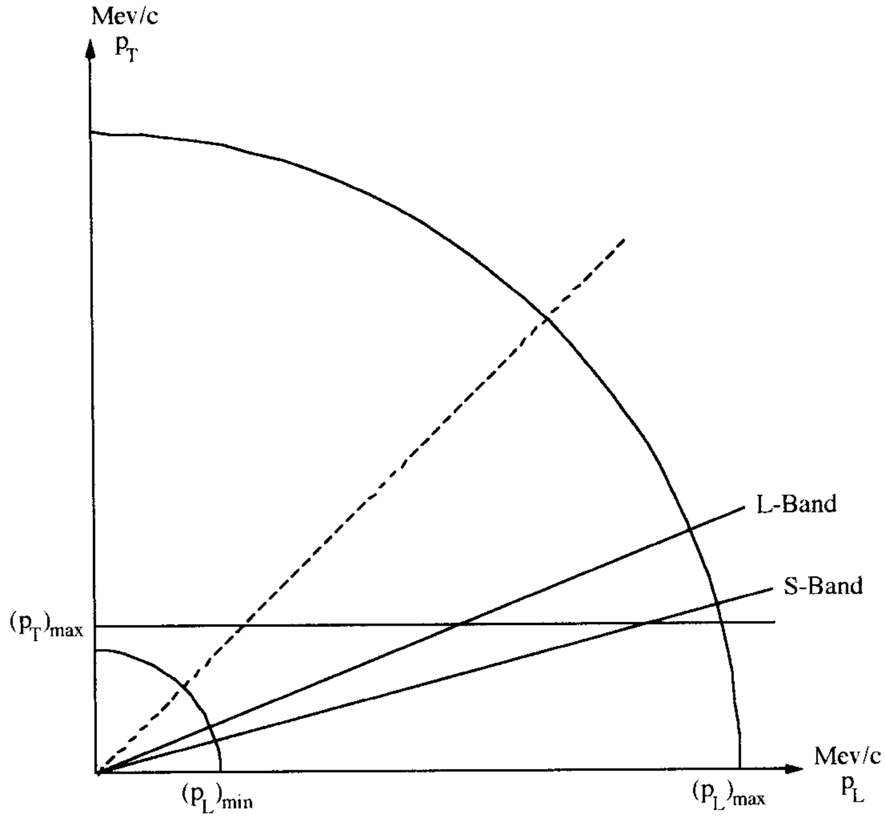

Figure 3.4.20: *Acceptance limitations for longitudinal and transverse momenta for two different choices of the injector frequency.*

Beam Loading

Exact calculations of the beam loading in the pre-accelerator with both electrons and positrons with different energies but with approximately the same transverse momenta is rather complicated. Simulations, using the RF characteristics of the chosen structure might shed some light on this important topic. Some studies have been started and results should appear in the near future. In the meantime we might expect some type of beam charge compensation to occur during the macropulse.

The Pre-Accelerating Structure

The positron pre-accelerator linac (3.2 GeV) would simply use superconducting L-band cavities such as those used for the main accelerator. However the optical characteristics of the positron beam emerging from the convertor preclude the use of a superconducting structure before the beam attains an energy of approximately 200 MeV. Therefore a copper structure is needed immediately behind the conversion target. As noted above, an L-band structure is preferred over a higher harmonic frequency from the point of view of positron acceptance and despite the loss of shunt impedance. The use of a normal conducting structure immediately raises the question of the maximum permissible accelerating gradient for 0.5 % duty cycles and the associated thermal dissipation problems. It is clear that the largest shunt impedance possible is desired in order to reduce cavity losses and to minimise the number of klystron- modulator assemblies required. A survey of copper accelerating structures indicates that a frequency scaled version of the MAMI injector linac structure [34] would be a good candidate for the positron pre-accelerator. This structure has a standing wave shunt impedance of 77 MΩ/m at 2445 MHz which indicates that we might achieve 56 MΩ/m at 1.3 GHz. Operation of the linac at a field of, say, 15 MV/m would then imply an average dissipation of 20 kW/m. Although this dissipation is slightly higher than that of the existing MAMI structure (15 kW/m continuous) it is no larger than the typical average power dissipation in single cell cw cavities used for electron storage rings (albeit at lower frequency). In addition, the smaller frequency of TESLA in comparison to MAMI and the resulting larger cavity dimensions, should easily allow increased cooling capabilities for an L-band version of the MAMI geometry. It should be noted that the problem of high power, long pulse operation of copper cavites might benefit from the existing studies being made for the TESLA RF gun which has to support a much higher field for the same pulse width and frequency. Operation at 15 MV/m implies a peak power of 4 MW/m. Consequently, the 10 MW klystrons currently under development for TESLA would comfortably feed two 1 m sections with 20% power in reserve. Six such klystrons would provide a positron beam of 180 MeV. One disadvantage of the MAMI structure is that its iris aperture, when scaled to 1.3 GHz is only 23 mm in diameter. This could seriously diminish the acceptance of the linac behind the matching device. Opening the iris would, in turn, reduce the shunt impedance, so requiring increased peak power for the same gradient. One could consider using increased aperture cells at the beginning of the pre- accelerator, followed by 23 mm apertures at an appropriate energy. Further cavity design work and simulation studies are needed here.

The 3 GeV positron pre-linac using standard TESLA cavities could start with doublet focussing between each cavity, yielding a beta function of about 1.5 m. The beam size at the entry of this linac would be $\sigma_{x,y}$=6 mm so that the iris aperture accomodates more than 5 standard deviations.

3.4.5.8 Low Intensity Auxiliary Source

For the commissioning of the positron damping ring, the main positron linac, etc., a source that works independent of the main electron linac would be desirable. Most of this work can be done or even has to be done at low intensities. Therefore a conventional low intensity source will be integrated into the high intensity source. An electron beam of only 500 MeV is sufficient to produce a few % of the design positron current using the thin Titanium target and the capture optics of the high intensity source. In this case the heat load of the target is high but does not reach the limits that have been previously discussed. The electron source for the low intensity positron source can also be used to provide electrons for the main linac for electron-electron and gamma-gamma collisions, respectively.

3.4.5.9 Potential Upgrade to a Polarized Positron Source

The proposed positron source allows also to produce polarized positrons as it was originally proposed by V. E. Balakin and A. A. Mickhailichenko [25, 24]. The technological demands are, however, much stronger in this case. Therefore the polarized source is regarded as a potential upgrade option.

In order to produce circularly polarized photons a short period helical undulator of about 100 m length has to be used instead of the planar wiggler. Since only the on-axis photons are completely circularly polarized off-axis photons have to be scraped off. This requires that the spot size of the photon beam on the target is dominated by the natural opening of the radiation rather than by the emittance contribution of the electron beam. Therefore the distance between the undulator and the target has to be increased to 150 m and the electron beam emittance has to be decreased to $\epsilon_x = 5 \cdot 10^{-10}$ m and $\epsilon_y = 10^{-10}$ m. The emittance requirements can easily be fulfilled for the vertical emittance, but can be achieved in the horizontal plane only with a strong collimation in the beam separation optics. Therefore only 60% of the electron beam can be matched to the undulator. Better results can be achieved if the horizontal β-function of the beams at the IP is increased with the disadvantage of some luminosity loss. Therefore improvements of the beam separation optics would be desirable. The parameters of the helical undulator are demanding and have not been reached so far. With a period length of 1 cm an on-axis field of 1.3 T has to be reached. These parameters can be realized only with superconducting technology at a gap radius of only about 2 mm. A detailed technological design of an undulator with the required parameters has not been worked out yet.

The polarization of the circularly polarized photons is transferred to the electron-positron pairs during pair production. For the calculation of the processes in the target the EGS4 code has been extended. The code includes polarization effects for pair production, bremsstrahlung and Compton scattering and yield a maximum longitudinal polarization of a polarized positron source of 50-60%.

Bibliography

[1] R. Alley et al., *The Stanford Linear Accelerator Polarized Electron Source*, Nucl. Instrum. And Meth. A365 (1995) 1.

[2] *Tesla Test Facility Linac – Design Report*, Ed.: D.A. Edwards, DESY Print, March 1995, TESLA 95-01.

[3] J.S. Fraser et al., Proc. of 1987 IEEE Particle Accelerator Conference, Washington DC, p. 1705.

[4] J. Clendenin et al., *Prospects for generating polarized electron beams for a linear collider using an RF gun*, Nucl. Instrum. And Meth. A 340 (1994) 133.

[5] K. Aulenbacher et al., *RF Guns and the Production of Polarized Electrons*, CLIC Note 303 and NLC-Note 20, May 1996.

[6] M. Woods et al., J. Appl. Phys. 73 (1993) 8531.

[7] A. Herrera-Gómez and W.E. Spicer, Proc. SPIE 2022 (1993) 51.

[8] D. Schultz et al., *The Polarized Electron Source of the Stanford Linear Accelerator Center*, SLAC-PUB-6606, August 1994; presented at 17th International Linear Accelerator Conference (LINAC 94), Tsukuba, Japan, 21-26 Aug 1994.

[9] H. Tang et al., *Experimental Studies of the Charge Limit Phenomenon in NEA GaAs Photocathodes*, SLAC-PUB-6515, June 1994; presented at 4th European Particle Accelerator Conference (EPAC 94), London, England, 27 Jun - 1 Jul 1994.

[10] P. Hartmann et al., *Picosecond Polarized Electron Bunches from a Strained Layer GaAsP Photocathode*, submitted to Nucl. Instrum. And Meth.

[11] J.E. Clendenin, *Polarized Electron Sources*, SLAC-PUB-95-6842, May 1995; Talk given at 16th IEEE Particle Accelerator Conference (PAC 95) and International Conference on High Energy Accelerators, Dallas, Texas, 1-5 May 1995.

[12] Although a conversion of the second or the third harmonic of the TTF laser system to 840 nm by optical parametric generation is in principle possible, it will be very difficult to achieve a reasonable efficiency to obtain the required laser energy per pulse.

[13] See e.g. W. Koechner, *Solid-State Laser Engineering*, Berlin, ^{4}1996, p. 400 ff.

[14] White et al., Opt. Lett. 17 (1992) 1067 and Ditmire, Perry, Opt. Lett. 18 (1993) 426.

[15] I. Will, P. Nickles, W. Sandner, *A Laser System for the TESLA Photo-Injector*, Internal Design Study, Max-Born-Institut, Berlin, October 1994.

[16] C. Travier, *On the Possibility of a Normal Conducting Photo-Injector for Tesla*, LAL/SERA/92-432, November 1992.

[17] B. Dunham, M. Jablonka, *Modeling of a High Charge Injector for the TESLA Test Facility*, DESY Print April 1994, TESLA 94-11.

[18] M. Breidenbach et al., *An inverted-geometry, high voltage polarized electron gun with UHV load lock*, Nucl. Instrum. And Meth. A 340 (1994) 1.

[19] C.K. Sinclair, *A 500 kV photoemission electron gun for the CEBAF FEL*, Nucl. Instrum. And Meth. A 318 (1992) 410.

[20] J.B. Rosenzweig et al., *Design of a High Duty Cycle, Asymmetric Emittance RF Photoinjector for Linear Collider Applications*, Proc. 1993 IEEE Particle Accel. Conf. 3021 (IEEE, 1994).

[21] K.J. Kim, Nucl. Instr. Methods A 275, 201 (1988).

[22] Warner Bruns, private communication.

[23] L. Serafini and J.B. Rosenzweig, *Envelope Analysis of Intense Relativistic Quasi-laminar Beams in RF Photoinjectors: A Theory of Emittance Compensation*, submitted to Phys. Rev. E.

[24] V. E. Balakin and A. A. Mikhailichenko, *The Conversion System for Obtaining High Polarized Electrons and Positrons*, Preprint INP 79-85, 1979.

[25] K. Flöttmann, *Investigations Toward the Development of Polarized and Unpolarized High Intensity Positron Sources for Linear Colliders*, DESY-93-161, 1993.

[26] R. Brinkmann, *Optimization of a Final Focus System for Large Momentum Bandwidth*, DESY-M-90-14, 1990.

[27] R. Brinkmann, J. Pflüger, V. Shiltsev, N. Vinokuro, P. Vobly, *Wiggler Options for TESLA Damping Ring*, DESY-TESLA-95-24, 1995.

[28] W. Nelson, H. Hirayama and D. Rogers, *The EGS4 Code System* SLAC-265, 1985.

[29] S. Ecklund, *Positron Target Materials Tests*, SLAC Collider Note-128, 1981.

[30] E. M. Reuter and J. A. Hodgson, *3D Nummerical Thermal Stress Analysis of the High Power Target for the SLC Positron Source*, SLAC-PUB-5370, 1991.

[31] P. Sievers and M. Höfert, *A Megawatt Electron Positron Conversion Target - A Conceptual Design*, Proc. European Accelerator Conference, Rom 1988.

[32] R. H. Helm, *Adiabatic Approximation for Dynamics of a Particle in the Field of a Tapered Solenoid*, SLAC-4, 1962.

[33] H. Ida, *Present R&D Status of Positron Sources for JLC-1 and ATF*, presented at Sixth International Workshop on Linear Colliders, Tsukuba 1995.

[34] Compendium of Scientific Linacs, CERN/PS 96-32, 1996.